Geophys. J. Int. (1998) **132,** 508–520

Surface-wave polarization data and global anisotropic structure

G. Laske and G. Masters
IGPP, Scripps Institution of Oceanography, La Jolla, CA 92093-0225, *USA*

Accepted 1997 September 7. Received in original form 1997 April 4

SUMMARY

In the past few years, seismic tomography has begun to provide detailed images of seismic velocity in the Earth's interior which, for the first time, give direct observational constraints on the mechanisms of heat and mass transfer. The study of surface waves has led to quite detailed maps of upper-mantle structure, and the current global models agree reasonably well down to wavelengths of approximately 2000 km. Usually, the models contain only elastic isotropic structure, which provides an excellent fit to the data in most cases. For example, the variance reduction for minor and major arc phase data in the frequency range 7–15 mHz is typically 65–92 per cent and the data are fit to within 1–2 standard deviations. The fit to great-circle phase data, which are not subject to bias from unknown source or instrument effects, is even better. However, there is clear evidence for seismic anisotropy in various places on the globe. This study demonstrates how much (or little) the fit to the data is improved by including anisotropy in the modelling process. It also illuminates some of the trade-offs between isotropic and anisotropic structure and gives an estimate of how much bias is introduced by neglecting anisotropy. Finally, we show that the addition of polarization data has the potential for improving recovery of anisotropic structure by diminishing the trade-offs between isotropic and anisotropic effects.

Key words: anisotropy, global tomography, path integral approximation, polarization, surface waves.

INTRODUCTION

Early inversions of surface-wave dispersion data showed that isotropic mantle models sometimes fail to explain both Love- and Rayleigh-wave phase data simultaneously (e.g. Schlue & Knopoff 1976). This 'incompatibility' led to the construction of transversely isotropic models on both a global scale (e.g. Dziewonski & Anderson 1981) and regional scales. Transverse isotropy has been found both on continents (e.g. Mitchell 1984) and in the oceans, especially the Pacific Ocean (Forsyth 1975; Schlue & Knopoff 1976; Regan & Anderson 1984; Yu & Mitchell 1979). The transversely isotropic layer is usually confined to be in the upper 200 km (e.g. Montagner & Anderson 1989) and a common observation is that transverse anisotropy is much stronger than azimuthal anisotropy.

Large-scale variations of azimuthal anisotropy appear to be quite well observed in the Pacific Ocean (Forsyth 1975; Nishimura & Forsyth 1989; Tanimoto & Anderson 1985; Suetsugu & Nakanishi 1987; Montagner & Tanimoto 1990). Most of these studies agree on the distribution of fast directions of Rayleigh-wave phase velocities. These tend to coincide with current spreading directions for young and intermediate-age oceans and with fossil plate motion directions for old oceans. Weaker azimuthal anisotropy is usually found in the very old oceans, which is explained by models having several anisotropic layers with different fast directions, for example when the current flow in the asthenosphere is not aligned with the direction of fossil plate motion in the lithosphere above.

From a geodynamical point of view, seismic velocities are expected to be anisotropic in some areas. For example, flow-induced anisotropy in the mantle is explained by the alignment of olivine crystals in an external finite strain field (lattice preferred orientation). If the strain field is coherent over a large area, the microscopic orientation of crystals should produce a macroscopically observable seismic signal. There are other processes which cause seismic anisotropy such as stacks of alternating isotropic layers, fluid or melt-filled cracks, etc. (Backus 1962; Crampin & Booth 1985; Kendall 1994), but these processes are thought to be responsible for anisotropy mainly in the crust. Azimuthal anisotropy of the compressional velocity in the uppermost mantle (constrained by observations of P_n traveltimes) is found to be of the order of up to 8 per cent in both continents and oceans (Fuchs 1983; Raitt *et al.* 1969). Azimuthal anisotropy of Rayleigh-wave phase velocity is generally observed to be smaller, for example less than 2 per

GJI000 17/2/98 16:38:46 3B2 version 5.20
The Charlesworth Group, Huddersfield 01484 517077

cent for 100 s Rayleigh waves (Montagner & Tanimoto 1990), but recent studies in the Pacific indicate that it might be as large as 6 per cent (Forsyth *et al.* 1996).

The trade-off between laterally isotropic velocity structure and anisotropy does not allow us to derive a unique phase-velocity model from our phase data. By inverting surface-wave phase data, Montagner & Tanimoto (1990, 1991) showed that azimuthal anisotropy is recovered on a global scale when it is included in the inversion, although it is not clear how much anisotropy is actually required to fit these data (Zhang & Tanimoto 1993). We find that isotropic phase-velocity maps usually provide an excellent fit to the data (Laske & Masters 1996). The variance reduction for minor and major arc phase data is typically 65–92 per cent in the frequency range 7–15 mHz and the data are fit to within 1–2 standard deviations. The variance reduction at higher frequencies is even greater (unpublished manuscript), although the initial χ^2 is also much larger. We believe that other types of data, such as measurements of the frequency-dependent arrival angle of incoming surface-wave packets (called polarization data hereafter), diminish some of the trade-offs and ought to be included in an inversion. Both phase and polarization are significantly affected by anisotropy (Maupin 1985; Vig & Mitchell 1990), but the greater impact is expected to be on polarization (Grünewald 1988). For example, Vig & Mitchell (1990) calculated that the anisotropy in the oceanic lithosphere causes off-azimuth arrival angles of up to 8° for 50 s Rayleigh waves.

INCLUDING ANISOTROPY IN THE MODELLING

In elastic, weakly anisotropic media (up to 10 per cent) the phase and group velocities can be described by a truncated trigonometric polynomial of degree 4 in Ψ, the azimuth, measured from the north. This formulation was originally derived for *P* waves (Backus 1965) and has been applied to surface waves by Smith & Dahlen (1973). As a first-order approximation, the frequency-dependent phase velocity at colatitude θ and longitude ϕ is

$$c(\theta, \phi, \Psi) = c_i(\theta, \phi) + a_1(\theta, \phi)\cos(2\Psi) + a_2(\theta, \phi)\sin(2\Psi) + a_3(\theta, \phi)\cos(4\Psi) + a_4(\theta, \phi)\sin(4\Psi), \quad (1)$$

where $c_i(\theta, \phi)$ is the azimuthally averaged velocity. The a_k are known linear functionals of the elastic parameters of the medium (Smith & Dahlen 1973; Montagner & Nataf 1986). It has been found that for any simple realistic petrological model (that is one symmetry axis which can be arbitrarily oriented), the contribution of the 4Ψ terms is relatively small for Rayleigh waves and that of the 2Ψ terms is small for Love waves (Smith & Dahlen 1973; Montagner & Nataf 1986). It is also expected that the effect of azimuthal anisotropy will, in general, be relatively small for Love waves (see also Schlue 1977; Kawasaki 1986), hence the examples shown here will concentrate on Rayleigh waves and we will ignore the 4Ψ terms.

We measure the frequency-dependent phase as the perturbation to the phase of a synthetic signal using the transfer function technique described in Laske & Masters (1996). The synthetic signal is computed using the reference 1-D model 1066a (Gilbert & Dziewonski 1975). For reasons of computational simplicity, the source–receiver great circle for each measurement is rotated to the equator so that longitude becomes the integration parameter:

$$\frac{\delta\Phi}{\Phi_0} = -\frac{1}{\Delta}\int_0^\Delta \frac{\delta c\left(\frac{\pi}{2}, \phi\right)}{c_0}\, d\phi, \quad (2)$$

where c_0 is the phase velocity of the reference model used to calculate the synthetics. We expand the local phase-velocity perturbation, $\delta c(\theta, \phi)/c_0$, in terms of surface spherical harmonics so that (2) becomes

$$\frac{\delta\Phi}{\Phi_0} = -\frac{1}{\Delta}\left[\sum_{l,m} c_{il}^m \int_0^\Delta Y_l^m\left(\frac{\pi}{2}, \phi\right) d\phi + \sum_{l,m} a_{1l}^m \int_0^\Delta Y_l^m\left(\frac{\pi}{2}, \phi\right)\cos(2\Psi)\, d\phi + \sum_{l,m} a_{2l}^m \int_0^\Delta Y_l^m\left(\frac{\pi}{2}, \phi\right)\sin(2\Psi)\, d\phi\right]. \quad (3)$$

We illustrate the retrieval of global azimuthal anisotropy using Rayleigh waves at 12 mHz. We obtain a global map of anisotropic phase velocity by measuring a large number of phase delays along great-circle arcs connecting sources and receivers. Our data set is that of Laske & Masters (1996) and includes 6200 data paths. In order to be able to compare the result to the previously published result for a purely isotropic map, we choose to truncate the expansion of $c_i(\theta, \phi)$ at $l = 16$, and those of $a_1(\theta, \phi)$ and $a_2(\theta, \phi)$ at $l = 12$. This gives 627 model parameters, which is comparable to the 625 parameters chosen for the azimuthally isotropic model (expansion up to $l = 24$) of Laske & Masters (1996). There is no particular weighting between the 0Ψ and 2Ψ terms, hence models with a high content of azimuthally dependent structure are not penalized or favoured. We use Occam's inversion scheme (Constable, Parker & Constable 1987), where we seek a smooth model which fits the data to within a given tolerance. In practice, there is some subjectivity in finding the optimal model. Here, the smoothing parameter is chosen in such a way that the spectrum of the 0Ψ term of the map is comparable in amplitude to that of the purely isotropic map. The result for the 0Ψ term is shown in Fig. 1. The patterns in the map appear to be very similar to those of the purely isotropic case. The regions with anomalously high phase velocity concentrate around the continental shield areas and the very old oceans, while low phase velocities are found along the mid-ocean ridges, the circum-Pacific system of subduction zones and the Afar Triangle–Red Sea region. The correlation is well above the 99 per cent confidence level, indicating that the anomalies of the two maps are in phase at all wavelengths. However, the spectral amplitudes at low harmonic degrees, especially at $l = 2$, seem to be significantly different. Also note that the amplitudes in the two spectra of the azimuthally dependent part in our anisotropic model are of the same order of magnitude as those of the 0Ψ term. From this one may conclude that improper treatment of anisotropy in the modelling process could lead to a biased picture of the Earth's (transversely) isotropic elastic properties, especially (and somewhat surprisingly) at long wavelengths. It is interesting to

GJI000 17/2/98 16:39:28 3B2 version 5.20
The Charlesworth Group, Huddersfield 01484 517077

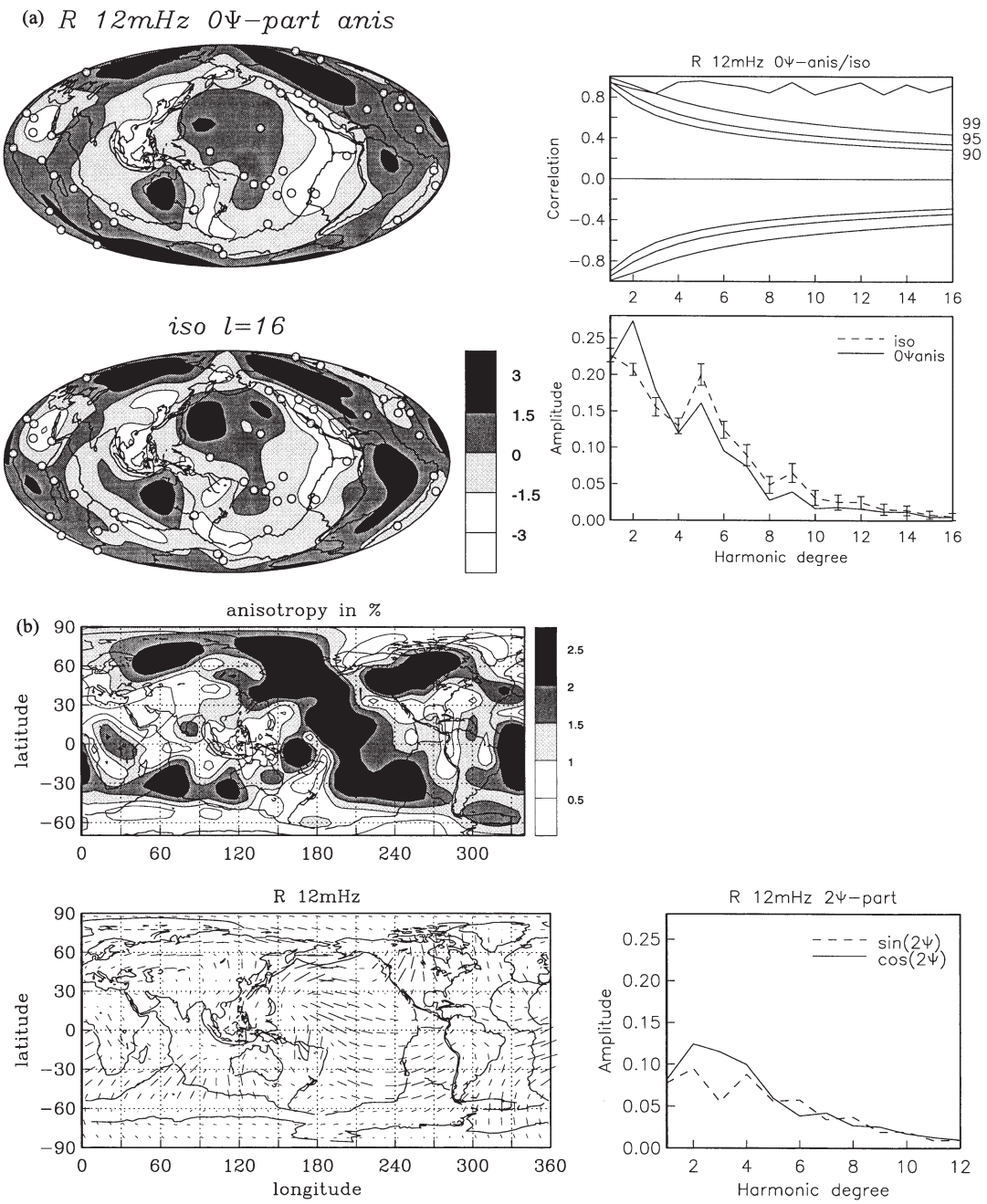

Figure 1. (a) (Left) Phase-velocity maps for Rayleigh waves at 12 mHz, obtained in an inversion using the phase data of Laske & Masters (1996). Lower panel: a purely isotropic map; upper panel: the 0Ψ part of an anisotropic map. The maps are perturbations, $\delta c/c_0$, to model 1066a (Gilbert & Dziewonski 1975), in per cent. These maps are expanded in surface spherical harmonics up to degree 16. (Right) Correlation and amplitude spectra. There is almost perfect agreement between the two maps in shape, and the correlation is well above the 99 per cent confidence level at all harmonic degrees. However, the amplitude spectra show significant differences at low harmonic degrees. (b) (Left) The azimuthally dependent 2Ψ part of the anisotropic phase-velocity map. This part of the model is expanded in spherical harmonics up to degree $l=12$. The top panel is the strength of anisotropy (the difference between the fastest and slowest velocity perturbation). Strong anisotropy can be found in the Pacific Ocean and North America. The anisotropy is never larger than 2.6 per cent. The bottom panel shows the direction of fastest velocity. Except for the old Pacific, the anisotropy found here is in agreement with that of Montagner & Tanimoto (1990). (Right) Amplitude spectra. Note that the contribution is quite large relative to the azimuthally independent term.

note that the $(c_i)_0^0$-coefficient, the global average of the phase-velocity anomaly with respect to the reference 1-D model 1066A, is unaffected by the inclusion of anisotropy. A change of this coefficient would indicate a trade-off between $(c_i)_0^0$ and other spherical harmonic coefficients, owing to poor data coverage.

The geographic distribution of the azimuthal dependence of anisotropy in our model is similar to the results of other studies. The fast directions generally agree with those found in the global studies of Tanimoto & Anderson (1985) and Montagner & Tanimoto (1991) and in studies of the Pacific (e.g. Suetsugu & Nakanishi 1987; Nishimura & Forsyth 1989).

GJI000 17/2/98 16:39:49 3B2 version 5.20
The Charlesworth Group, Huddersfield 01484 517077

Table 1. Variance reductions (in per cent) and misfit (χ^2/N) for individual data set and models. GC refers to great-circle phase data. The lower table shows the results for R_1 phase data and polarization data at stations PPT (Papete, Tahiti) and KIP (Kipapa, Hawaii).

	Model	R_1-Phs	R_2-Phs	GC-Phs	Pol
iso	ISO	88/2.4	86/1.5	81/0.9	35/1.9
anis (phase only)	AMOD.g	91/1.8	87/1.4	82/0.9	10/2.6
AMOD.g; 0Ψ only	AMOD.g0	82/3.5	80/2.0	71/1.4	12/2.5
anis (phase + polar.)	AMOD.gp	88/2.3	86/1.4	80/1.0	35/1.9
		PPT-Phs	PPT-Pol	KIP-Phs	KIP-Pol
	ISO	84/3.5	52/1.7	72/2.8	37/1.7
	AMOD.g	91/1.9	28/2.5	79/2.1	−24/3.4
	AMOD.gp	88/2.6	54/1.6	77/2.3	41/1.6

They tend to coincide with the direction of absolute plate motion and are roughly perpendicular to most of the mid-ocean ridges. The magnitude of anisotropy $[(c_{fast}-c_{slow})/c_0]$ is less than 2.5 per cent, which is slightly higher than in other global studies. From Table 1 it can be seen that both maps, ISO and AMOD.g, fit the data equally well, though the data for R_1 are slightly better fit by the anisotropic model. Of all the phase data, the R_1 data are the most sensitive to short-wavelength structure and anisotropy.

Table 1 also indicates that neither model fits the data to within their estimated errors but our attempts to find better-fitting models lead to both isotropic and anisotropic models with spectra that are oscillatory: odd-order structure tends to be much larger than even-order structure. We believe this to be an artefact of the way most phase data average structure and not a feature of the real Earth.

A preliminary conclusion from these experiments is that it remains unclear if azimuthal anisotropy is actually required by the phase data. Including anisotropy in the inversions seems to produce sensible models but does not provide a significant improvement in fit to the data. Since the results shown here provide key information about how mantle flow could be arranged within the Earth, it is essential to either confirm or refute these findings using other seismic constraints.

THE BIAS CAUSED BY IGNORING ANISOTROPY

In order to estimate the bias introduced by (not) including anisotropy in the inversion process, we perform a case study with three tests. In the first test (test A), a synthetic data set is created with the anisotropic map AMOD.g of Fig. 1. This data set is used to invert for an anisotropic map where the same smoothing constraint and parametrization are used as in the inversion of the real data. This test shows how the smoothing constraint and the error distribution in the data set control the bias in the resulting phase-velocity map. In the second test (test B), the data set created in test A is used in an inversion for a purely isotropic map (0Ψ part only). This test helps to estimate the bias introduced when not including anisotropy in the modelling process. Finally, in test C, we create synthetic data using only the 0Ψ part of map AMOD.g. This data set is used in an inversion for an anisotropic map. Test C reveals how much of the purely isotropic structure could be erroneously mapped into azimuthally dependent structure. We are especially interested to see if the alteration of the isotropic input map by this process is significant.

If the data coverage was perfect and errors small, the regularization of the inversion could be relaxed so that the resulting map would be unbiased. The chosen smoothing constraint suppressed artefacts in places of poor data coverage but it also increased the final data misfit, χ^2/N. Strong smoothing could map short-wavelength structure into longer wavelengths and, perhaps, from one set of spherical harmonic coefficients into another. In test A, we are particularly interested in how much structure of the 0Ψ part could be mapped into the 2Ψ part, or vice versa. The maps of the 0Ψ and 2Ψ parts of the output map are virtually identical to those of the input map (Fig. 1), hence we want to concentrate on a quantitative comparison in Fig. 2. The amplitude spectra of all three sets of spherical harmonic coefficients (c_i, a_1 and a_2) of the original map are generally well recovered, although the amplitudes in the output sets are somewhat smaller at high harmonic degrees l. The decreased amplitude of the output map at high l is a well-understood effect of the chosen smoothing constraint (rough models, hence large amplitudes at high l are penalized). Since Table 2 indicates an excellent fit to the data by the new map, the discrepancy in the amplitude spectra of Fig. 2 suggests that the phase data set may be somewhat insensitive to small changes in the spectral amplitudes at high harmonic degree (see also Laske & Masters 1996). On the other hand, the correlation between input and output maps is well above the 99 per cent confidence level at all harmonic degrees for all three sets of spherical harmonic coefficients (c_i, a_1 and a_2). This demonstrates that there is no significant mapping of 2Ψ structure into 0Ψ structure, or vice versa.

Table 2. Variance reductions (VR) and misfit (MF = χ^2/N) for the synthetic data sets and the three test models. The input map to create the data for tests A and B is anisotropic, while that for test C is isotropic. Note that in test C, the azimuthally dependent part is actually required to fit perfectly the synthetic data.

	Test A	Test B	Test C	
input	anisotropic	anisotropic	isotropic	
output	anisotropic	isotropic	anis (0Ψ) only	anisotropic
VR	99.9%	97.6%	98.9%	99.9%
MF	0.02	0.4	0.2	0.02

GJI000 17/2/98 16:39:53 3B2 version 5.20
The Charlesworth Group, Huddersfield 01484 517077

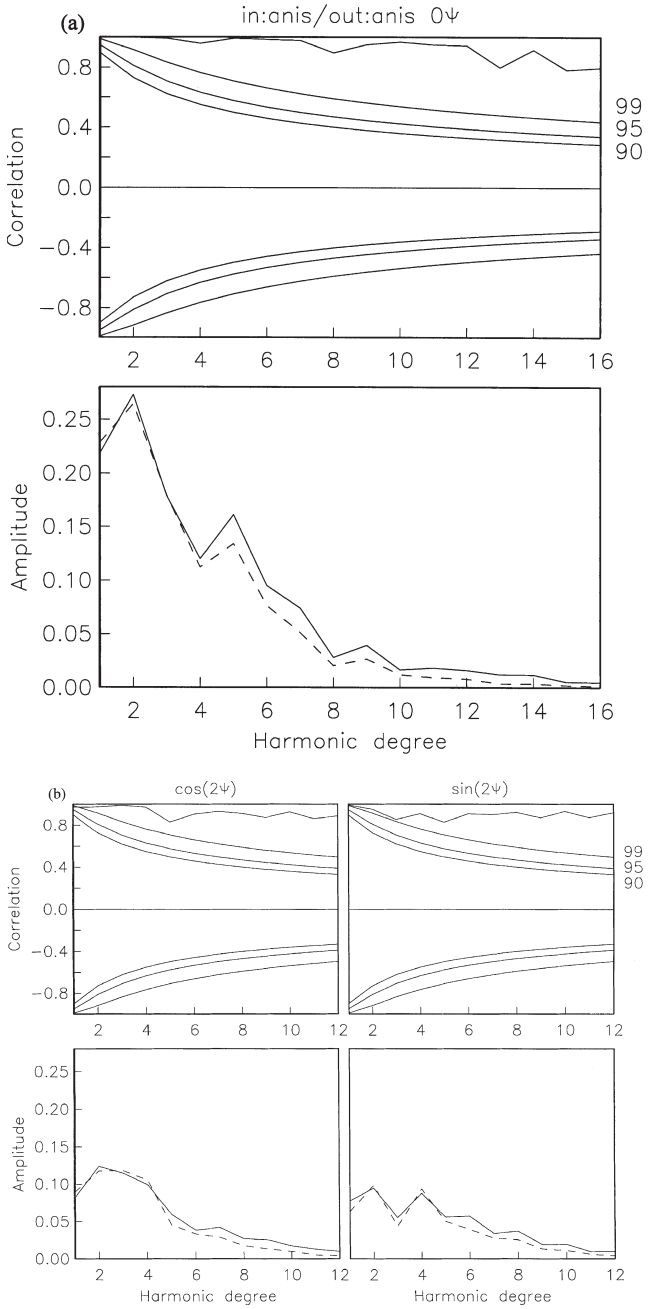

Figure 2. Comparison of the spectra of input and output model for test case A. Input: anisotropic model, solid line; output: anisotropic model, dashed line. (a) is the 0Ψ part, while (b) shows the azimuthally dependent 2Ψ part. The agreement is excellent. The output model has slightly reduced amplitudes for all three sets of harmonic coefficients, c_i, a_1, a_2, which is caused by the regularization of the inversion.

In test B, the data set of test A is used in an inversion for a purely isotropic map. The correlation between the resulting map and the 0Ψ part of the input map is remarkably good, although it sometimes drops below the 99 per cent confidence level (Fig. 3). Somewhat surprisingly, the amplitudes, especially at low harmonic degrees (e.g. $l=2$), are rather different from those of the input map. This discrepancy may be as large as the error bars determined for the spectra when using real data (compare with Fig. 1), hence the bias caused in this

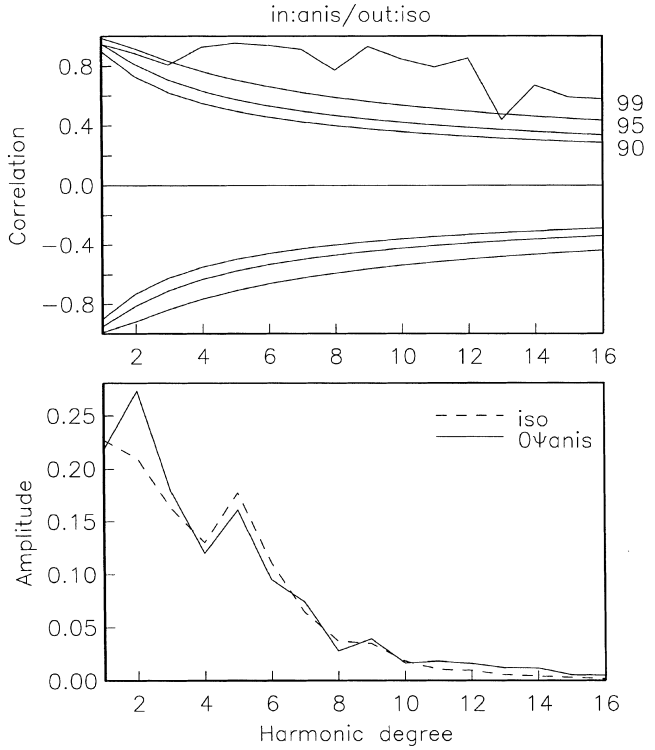

Figure 3. Comparison of input and output model for test case B (input: anisotropic model; output: isotropic model), except at $l=13$. The models agree well in shape, the correlation is well above the 99 per cent confidence level. The amplitude spectra reveal disagreement at low harmonic degrees, especially at $l=2$.

particular case may be significant. The observed effect is highly reproducible and also occurs if the synthetic data are created using only long-wavelength anisotropic structure (2Ψ term truncated at $l=6$). This suggests a rather weak trade-off between short-wavelength azimuthally dependent structure and long-wavelength azimuthally independent structure. The fit to the data is somewhat poorer for the isotropic output map of this test than the anisotropic output map of test A (Table 2), which may also indicate that the signal produced by azimuthally dependent structure cannot be simply explained by purely isotropic structure, even if short-wavelength structure is included in the modelling process. It is interesting to note that, for the real data, the greatest discrepancy between the isotropic map and the 0Ψ part of the anisotropic map is also at $l=2$. The results of experiment B may indicate that models obtained in an inversion for isotropic phase-velocity maps might be slightly biased if extremely long-wavelength large-amplitude azimuthal anisotropy is present.

In test C, we use only the 0Ψ term of the anisotropic map AMOD.g to create new synthetic data and invert for an anisotropic map. This test shows how much of the signal of an azimuthally isotropic map would be mapped into non-existent anisotropic structure. Fig. 4 reveals that the azimuthally independent structure is well recovered. The amplitude of the 0Ψ term is somewhat reduced at higher l, but this could also be caused by the chosen regularization (see results of test A). The spectral amplitudes of the azimuthally dependent part of the resulting map appear to be negligibly small. Surprisingly, this part of the map is actually required to fit perfectly the data (Table 2). This suggests some mapping of azimuthally

GJI000 17/2/98 16:39:58 3B2 version 5.20
The Charlesworth Group, Huddersfield 01484 517077

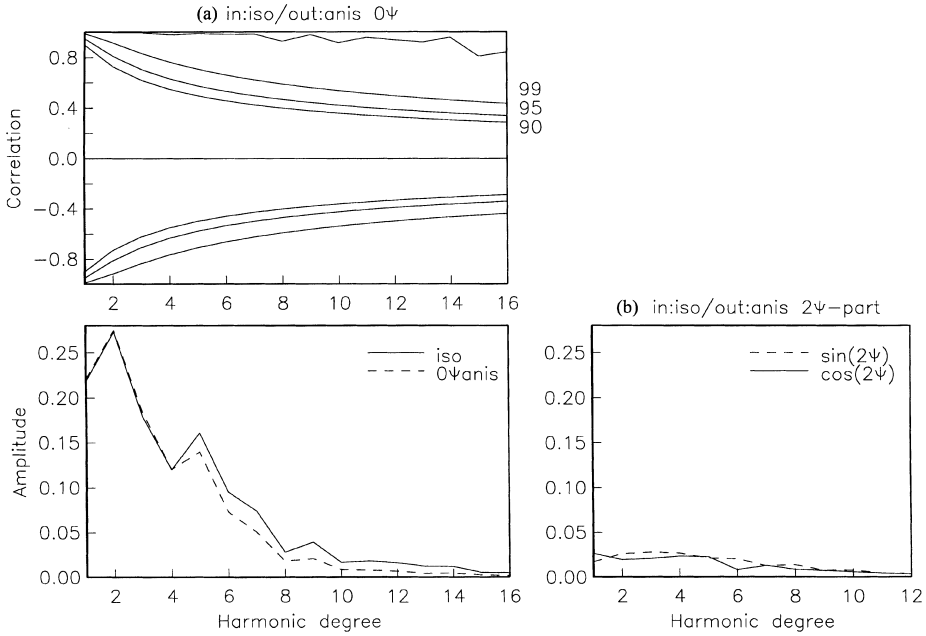

Figure 4. Comparison of input and output model for test case C (input: isotropic model; output: anisotropic model). Again, the models agree well in shape, and the amplitude of the 0Ψ part (a) is only slightly smaller at higher harmonic degrees than those of the input model. (b) shows the spectra of the 2Ψ part of the output model.

isotropic structure into the 2Ψ part which is introduced by our smoothing constraint. With very little damping (which is not desirable with real data), the amplitudes of the azimuthally dependent part are practically zero.

This experiment, together with test B, has shown that the bias introduced by including non-existent anisotropy in the modelling process appears to be small, though the amplitudes of short-wavelength azimuthally averaged structure might be slightly underestimated. On the other hand, ignoring existing anisotropy may result in a biased model of the azimuthal average of phase velocity structure. One may conclude from this that anisotropy should be included in a global inversion. However, the higher number of degrees of freedom requires a stricter choice of damping in the inversion. Our particular choice of regularization, where we search for smooth models, may lead to too smooth global phase-velocity maps. Perhaps an ideal inversion would include short-wavelength azimuthally averaged structure but only long-wavelength azimuthally dependent structure. However, note that the spectral amplitude of the azimuthally dependent part seems to roll off rather slowly with increasing wavenumber (Fig. 1).

CONSTRAINTS FROM POLARIZATION DATA

Laske & Masters (1996) have shown that polarization data (arrival angle of incoming wave packets) can be extremely useful in resolving the short-wavelength structure of an isotropic phase-velocity map. Ray-tracing experiments demonstrate the potential of such a data set for recovering anisotropic structure (Figs 5 and 6). We implemented a 'shooting'-type ray tracer based on the theoretical results of Tanimoto (1987) and shot rays through both the isotropic and anisotropic maps (ISO, AMOD.g) using the geometry of our actual data. The predicted phase data for the isotropic and anisotropic maps are well correlated (Fig. 5) but the polarization angles can change quite dramatically after adding dominantly long-wavelength anisotropic structure to the model (Fig. 6). Note that the phase is also affected by anisotropy for very short travel paths, and so has the potential to constrain anisotropy. Unfortunately, reliable phase measurements for short paths are difficult to obtain since overtones are likely to contaminate the arriving wave train.

In order to be able to include polarization data in the modelling, we need a formalism to interpret these angles. By using linear perturbation theory, Woodhouse & Wong (1986) showed that the dependence of the tangent of the observed arrival angle, v, on local isotropic phase-velocity heterogeneity can be expressed by the path integral along the great-circle arc joining source and receiver (Fig. 7). Mochizuki (1990) has extended this path integral approximation (PIA) to include weak anisotropy. The linear relationship between v, now being the tangent of the group arrival angle, and the weakly anisotropic and heterogeneous local phase velocity is

$$v(\Delta) = -\left.\frac{d\gamma}{d\phi}\right|_{\phi=\Delta} - \frac{1}{\sin\Delta}\int_0^{\Delta} \sin\phi(\partial_\theta + \partial_\phi\partial_{\psi_s})\frac{\left(\frac{\pi}{2},\phi\right)}{c_0}\,d\phi, \quad (4)$$

where the great circle has been rotated to be along the equator with the source at longitude $\phi = 0$ and the receiver at epicentral distance $\phi = \Delta$ and $\gamma = \cot\theta$ (Fig. 5). ∂_θ, ∂_ϕ, ∂_{Ψ_s} are the derivatives with respect to the coordinates and the azimuth of the wavenumber vector, Ψ_s, measured from the south. c_0 is the average phase velocity of the Earth. This equation shows that the arrival angles depend on gradients of phase velocity rather than phase velocity itself, and so are intrinsically more sensitive to shorter-wavelength heterogeneity and anisotropy than phase data are.

Ray-tracing experiments using the anisotropic phase-velocity map we obtained for Rayleigh waves at 12 mHz

GJI000 17/2/98 16:40:02 3B2 version 5.20
The Charlesworth Group, Huddersfield 01484 517077

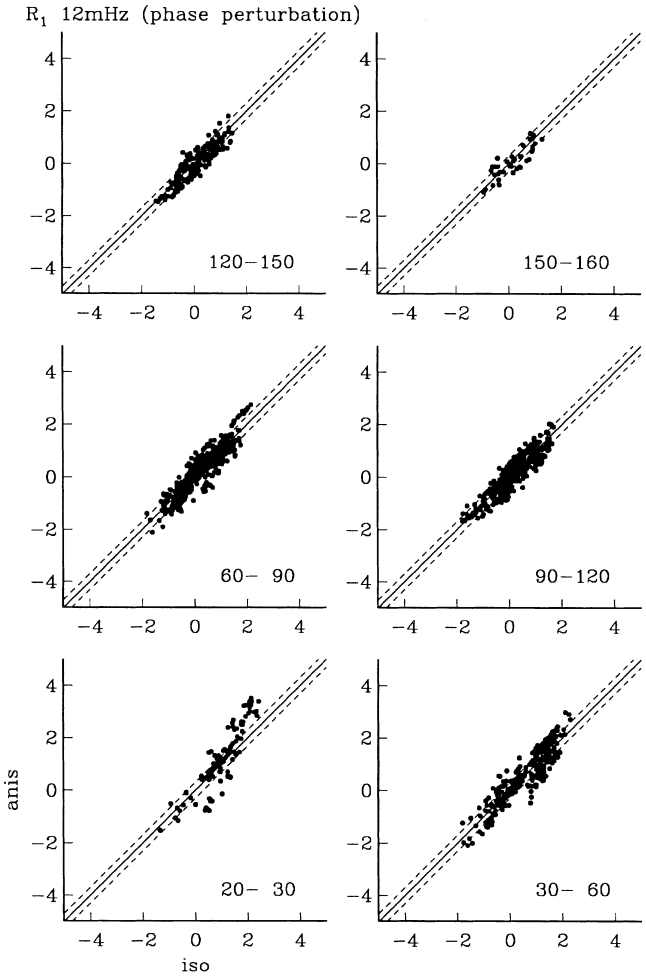

Figure 5. Correlation of phase perturbations (with respect to model 1066a, in per cent) obtained with ray tracing using the isotropic and anisotropic maps of Fig. 1. The numbers in the corners indicate various epicentral distance ranges. The dashed lines are the minimum errors in the measurements (0.4 per cent). Note that the changes are barely significant, except for data with short travel paths.

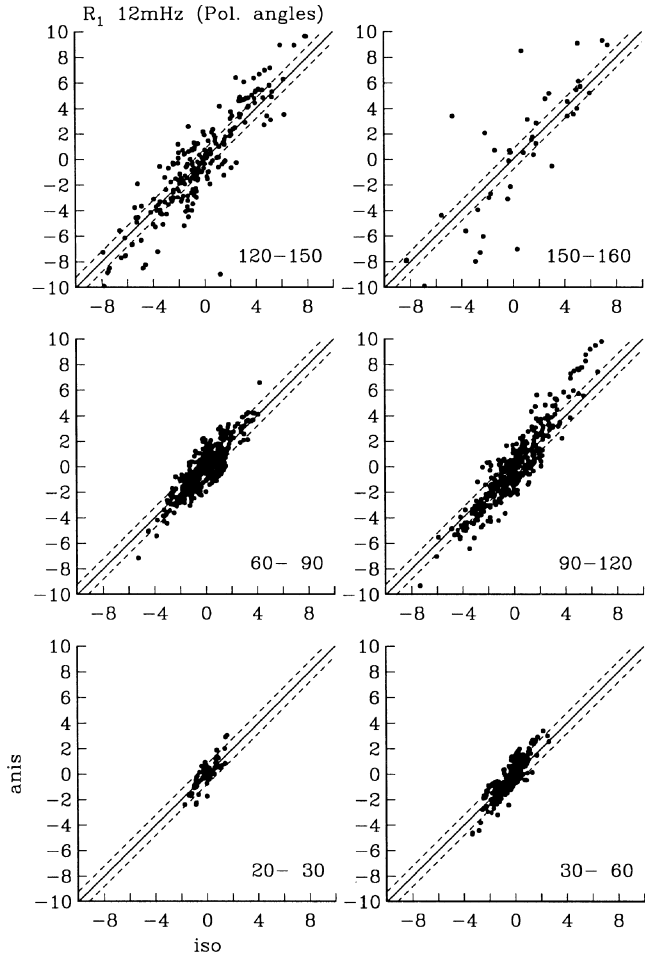

Figure 6. Correlation of arrival angles obtained with ray tracing using the isotropic and anisotropic maps of Fig. 1. Arrival angles at distances close to 160° are less certain because the receiver may be located in a ray caustic. The dashed lines indicate the minimum measurement error (1°).

(AMOD.g of Fig. 1) are very encouraging and suggest that the PIA may be adequate to interpret our observed arrival angles. Fig. 8 shows a comparison for 1800 minor arc paths which make up 72 per cent of our entire polarization data set. Apart from very few angles at larger epicentral distance, the difference of the angles predicted by the PIA and ray tracing is less than 1.0°, which is about as well as polarization angles can be measured. At greater epicentral distances, the rays are more likely to pass antipodal caustics where ray theory breaks down. Tests with models having only one non-zero model parameter suggest that the linear approximation breaks down if the coefficients are 10 times as large as they are expected to be in a realistic map for global anisotropic phase velocity.

In order to demonstrate the potential for enhancing the resolution of an inversion by including the polarization data, we perform a test similar to the checkerboard test of Laske & Masters (1996). This test gives an idea of the geographic distribution of the distortion of a map with our current data coverage. We use the same generalized inverse matrix (same data coverage and smoothing constraint) as we would use for producing our map from the real data (see Laske & Masters 1996 for details). The coefficients in the input map are all zero except for the sin (2Ψ) coefficient $\mathcal{R}e(a_2)_8^4$. If only phase data are used in the inversion, the pattern of the strength of anisotropy

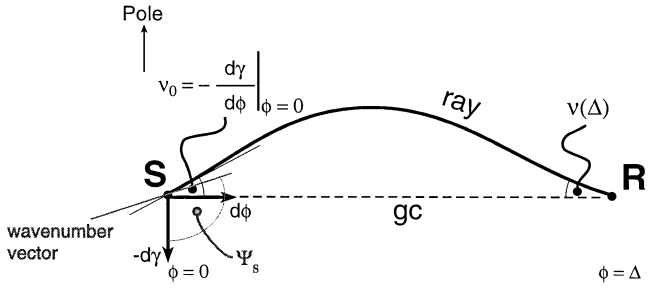

Figure 7. Ray geometry of a true ray for surface waves from the source (S) to the receiver (R) through a weakly anisotropic and heterogeneous medium. For convenience, the great circle (GC) has been rotated onto the equator. ν is the tangent of the measured polarization angle. θ and ϕ are colatitude and longitude, with $\gamma = \cot\theta$ (Woodhouse & Wong 1986). Ψ_S is the azimuth of the wavenumber vector, measured from the south.

GJI000 17/2/98 16:40:22 3B2 version 5.20
The Charlesworth Group, Huddersfield 01484 517077

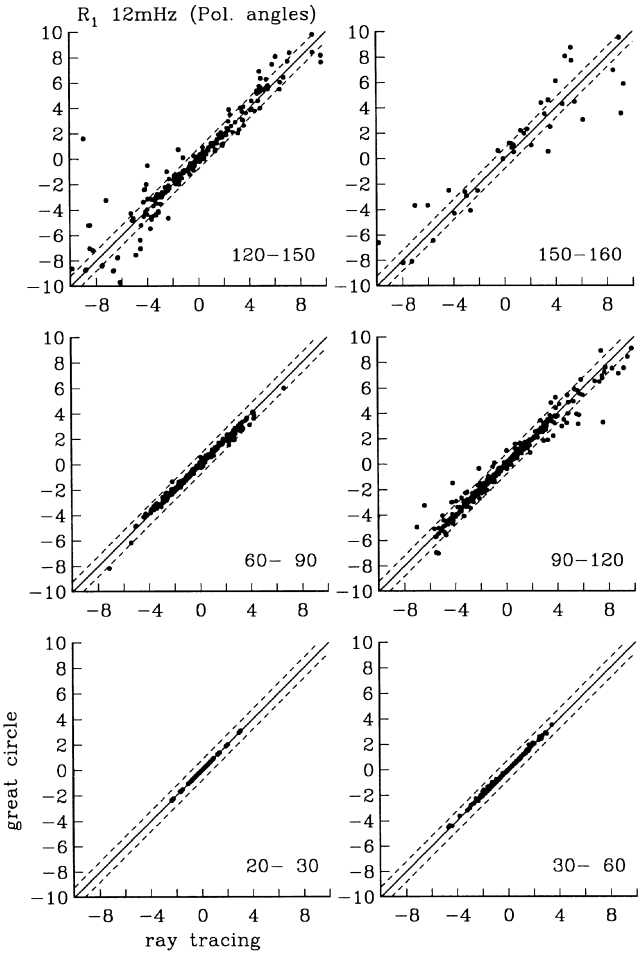

Figure 8. Correlation of arrival angles obtained with ray tracing and the linear path integral approximation. In most cases, the differences are not significant. Arrival angles predicted at distances close to 160° are less certain because the receiver may be located in a ray caustic.

is sufficiently well recovered only in areas with excellent data coverage, which is the area along the rim of the Pacific Ocean (Fig. 9). In the Pacific Ocean itself, pattern recovery is poor. The resolution is dramatically improved after adding the polarization data to the inversion process. In general, the direction of the fastest velocity is well recovered, except for some areas including the southeastern Pacific and northwestern Atlantic. Note that the greyscale in the plot of the strength of anisotropy is different for the input and output maps. The recovery of the peak amplitude of the strength of anisotropy (compare upper panels of Figs 9a, b and c) is only 63 per cent in both cases. As already mentioned in the previous section, the recovery of the spectral amplitude of the map is relatively poor at high harmonic degree. A considerable part of the input coefficient at $l=8$ is smeared into coefficients at other harmonic degrees (Fig. 9d), and the recovery is only 46 per cent (phase only) and 50 per cent (phase and polarization). It is also the case that there is considerable smearing into the other two sets of coefficients [0Ψ and $\cos(2\Psi)$]. However, Fig. 9(d) also reveals that the smearing is much less if polarization data are included. A better data coverage will certainly help to diminish this deficiency. This test is thought to represent an extreme case. Not surprisingly, the recovery of a $l=6$ pattern is much better (not shown). A coefficient $\mathcal{R}e(a_2)^3_6$ is recovered at the 65 per cent level. It is also true that in this case, the addition of polarization data does not lead to an improvement of resolution as much as it does for the $l=8$ pattern. However, the polarization data are also needed in this case to diminish the smearing of energy into lower harmonic degrees (especially, and somewhat surprisingly, $l=1$).

A PRELIMINARY INVERSION USING POLARIZATION DATA

A preliminary inversion including the polarization data measured at 76 global stations (Laske & Masters 1996) yields a rather puzzling map (AMOD.gp). In the following, we will concentrate on the azimuthally dependent part (2Ψ term, Fig. 10). In most areas, only small changes of map AMOD.g are necessary to give much better fits to the polarization data (AMOD.gp) (Table 1). This is not true for the areas around some stations in the Pacific Ocean [e.g. KIP (Hawaii), PPT (Papete, Tahiti)] and along the East Pacific Rise (compare with Fig. 1). In map AMOD.g (phase data only), the fast direction at station KIP was basically aligned with the present direction of plate motion, whereas in map AMOD.gp, the fast direction is almost perpendicular to the one in AMOD.g and is in a northeasterly direction. The strength of anisotropy is also reduced significantly. Since effects like these are observed only in a few areas, a mistake in the inversion scheme is rather unlikely. Both phase and polarization data can be influenced by strong 'local' effects such as topography (Maupin 1987) and we may have to correct the data for such effects (e.g. Snieder 1986). However, since the same phenomenon is also observed at longer periods (e.g. 150 s), a strong bias due to topography seems unlikely. Other effects, for example instrumental effects and misorientation, can be ruled out. A combined inversion of the polarization data for phase-velocity structure and instrument misorientation detected a possible alignment error of less than 2° at KIP (Laske 1995). It is also interesting that the phase data at KIP are practically equally well fit by AMOD.g and AMOD.gp, while the fits to the polarization data are quite different (Table 1, Fig. 11). While the purely isotropic map of Laske & Masters (1996) (ISO) and map AMOD.gp produce rather similar patterns in the distribution of arrival angles at station KIP, the predictions of map AMOD.g are clearly inconsistent with the data. Data collected at other stations (e.g. PPT) do not show as strong an inconsistency as found for KIP.

While the new model (AMOD.gp) may be counter-intuitive, our result supports the Hawaiian swell model of Phipps Morgan (personal communication, 1996) in which the flow direction in the mantle under the lithosphere would be perpendicular to the Hawaiian chain axis. Our observations are also consistent with results from some studies on *S*-wave splitting in this area (Ansel & Nataf 1989; Vinnik, Farra & Romanowicz 1989), although direct comparison is somewhat difficult owing to the different sampling depths of *S* waves (with almost vertical incidence) and surface waves. Results like these have to be confirmed or refuted by a more comprehensive study before further interpretation is possible. However, this experiment emphasizes the great potential of polarization data to constrain the global distribution of azimuth-dependent phase velocity better.

GJI000 17/2/98 16:40:34 3B2 version 5.20
The Charlesworth Group, Huddersfield 01484 517077

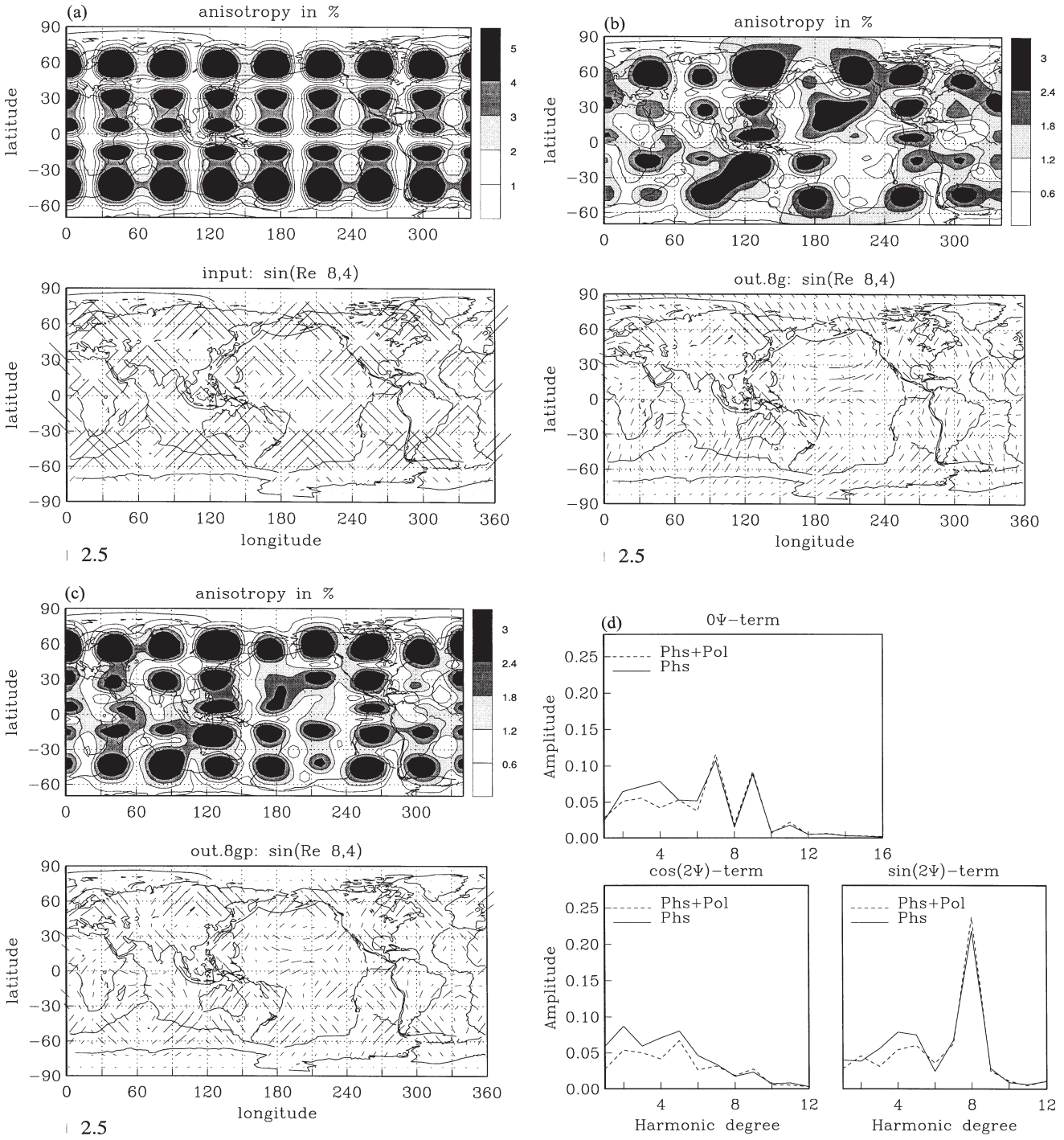

Figure 9. Resolution test using a map where only the sin(2Ψ) coefficient $\mathscr{R}e(a_2)_8^4$ is non-zero. We show only the azimuthally dependent part (2Ψ term). This test assumes that non-linear effects are unimportant and proceeds by inverting a synthetic data set using the same inverse matrix (same data coverage, error distribution and smoothing) that is used to invert the real data. (a) Input model. (b) The recovery of the pattern when only phase data are used. (c) The recovery when polarization data, measured at 76 global stations, are also included. The quality of recovery is improved tremendously when polarization data are added. (d) The amplitude spectra for both output maps (Phs: phase only; Phs+Pol: polarization data included). The amplitude of the input peak at $l=8$ was 0.48.

CONSTRAINTS ON ANISOTROPY FROM OTHER OBSERVATIONS

It is important to note that, in anisotropic media with arbitrarily oriented symmetry axes, we can no longer observe pure Rayleigh- and Love-wave signals. For example, the coupling of surface waves due to anisotropy results in elliptically polarized quasi-Love waves (Crampin 1975). When we measure polarization, we measure more than just the apparent arrival angle. In fact, we measure the complete orientation of particle motion including ellipticity and 'dip' (which measures how much a 'Love wave' appears on a

GJI000 17/2/98 16:40:38 3B2 version 5.20
The Charlesworth Group, Huddersfield 01484 517077

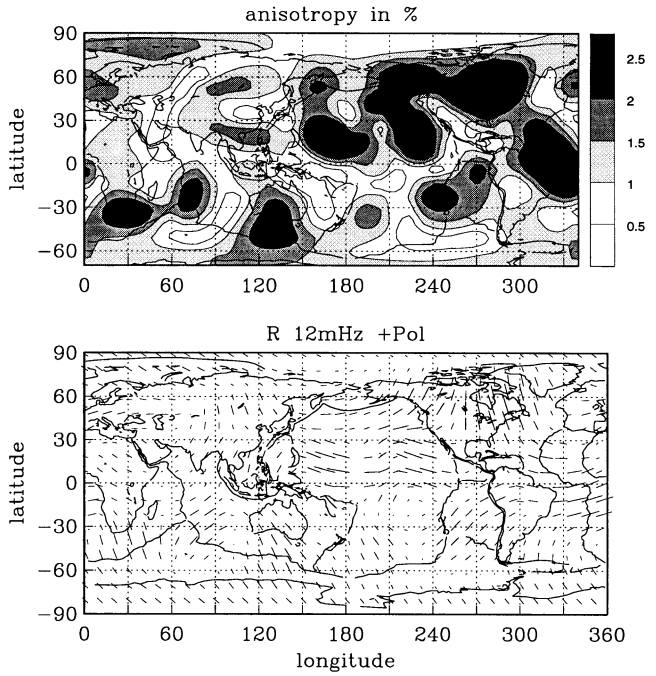

Figure 10. The azimuthally dependent part (2Ψ part) of the anisotropic phase-velocity map obtained when polarization data are included in the inversion. For details see Fig. 1(b). In some areas, especially around Hawaii, the orientation of the fast direction changes completely.

vertical-component recording). There is evidence at a few stations that the particle motion of clean Love-wave signals is not linear but elliptical. A 'clean' signal is detected by our multitaper method if its particle motion can be described by an elliptical motion which is confined to a plane (Laske, Masters & Zürn 1994). Here, the linear particle motion of Love waves in isotropic media is a special case. However, we have not yet found clear evidence for a systematic behaviour of particle motion ellipticity even in regions in the Pacific Ocean where we can expect uniform anisotropy.

At stations KIP and PPT the 'dip', the deviation from the horizontal, can be 20°, but most of the data lie within 5° (for Love waves at 12 mHz). For Rayleigh waves at the same frequency, the deviation from the vertical is also less than 20° (most data scatter around 10°). At other stations (e.g. INU, Inuyama, Japan) this angle is much greater, although the errors are also greater (the average deviation from the vertical is 20°). Measurements of 'Love waves' on vertical components have been made by Park and co-workers (e.g. Park & Yu 1992; Yu & Park 1994), who make a convincing argument for strong anisotropy in the South Pacific. Measurements of general particle motion orientation have also been used by Vig & Mitchell (1990) in a study of anisotropy beneath Hawaii. In areas where even small lateral gradients in azimuthal anisotropy are expected, observations such as the frequency-dependent dip should be extremely helpful to remedy the trade-off between anisotropic and isotropic velocity structure.

DISCUSSION

We have pointed out that isotropic phase-velocity maps (azimuthally averaged phase velocity) can explain most of the signal in our phase data. Azimuthal anisotropy can significantly affect such data, and including anisotropy in the modelling process gives additional variance reduction. However, the improvement of the fit to the data is small, despite the tremendous increase in the number of model parameters. The procedure for choosing the final model is rather subjective and a similar improvement could probably be achieved by choosing a rougher isotropic model. With our current data set, not including anisotropy in the modelling process may lead to biased results for the azimuthally averaged phase velocity at very long wavelengths, especially at harmonic degree 2. However, this bias is smaller than the differences introduced by the choice of inversion schemes of various workers (Table 3; see also Fig. 10 of Laske & Masters 1996). At this point, it remains unclear if phase data alone require azimuthal anisotropy to be well fit.

Seismic anisotropy also significantly affects surface-wave arrival angles. Our tests have demonstrated the great potential of such data to resolve azimuth-dependent phase velocity better. The preliminary inversion including our polarization data leads to a rather puzzling model. Some of the features in this map have not been seen in previous surface-wave studies and might be artefacts, owing to incomplete data coverage, some inconsistencies in the data set (the final misfit is greater than 1), and unmodelled effects (e.g. topography). However, owing to the different sensitivity of the polarization data to anisotropic structure, such data are capable of resolving structures which are averaged out by the phase data.

Table 3. The c_2^m coefficients of the isotropic phase velocity map of Laske and Masters (1996) for Rayleigh waves at 12 mHz. The numbers below are differences between these coefficients and those of various other models. ANIS: 0Ψ term of anisotropic map (this study); M&T: Montagner & Tanimoto (1991); T&W: Trampert & Woodhouse (1995); ET&L: Ekström, Tromp & Larson (1997); Z&L: Zhang & Lay (1996). The effect of the Earth's hydrostatic ellipticity (Woodhouse & Dahlen 1978) was added back to the c_2^0 coefficient of T&W and Z&L, since ellipticity was included in their modelling.

Model	c_2^0	$\mathscr{R}e(c_2^1)$	$\mathscr{I}m(c_2^1)$	$\mathscr{R}e(c_2^2)$	$\mathscr{I}m(c_2^2)$
ISO	0.67 ± 0.03	0.42 ± 0.02	-0.36 ± 0.02	0.56 ± 0.02	0.72 ± 0.02
ANIS	0.48	0.05	0.02	0.39	−0.33
M&T-ISO	−0.06	0.06	0.00	0.20	−0.09
T&W-ISO	0.19	−0.20	−0.18	0.07	−0.30
ET&L-ISO	0.22	−0.04	−0.36	0.19	−0.05
Z&L-ISO	−0.17	−0.10	0.09	−0.10	−0.24

GJI000 17/2/98 16:40:41 3B2 version 5.20
The Charlesworth Group, Huddersfield 01484 517077

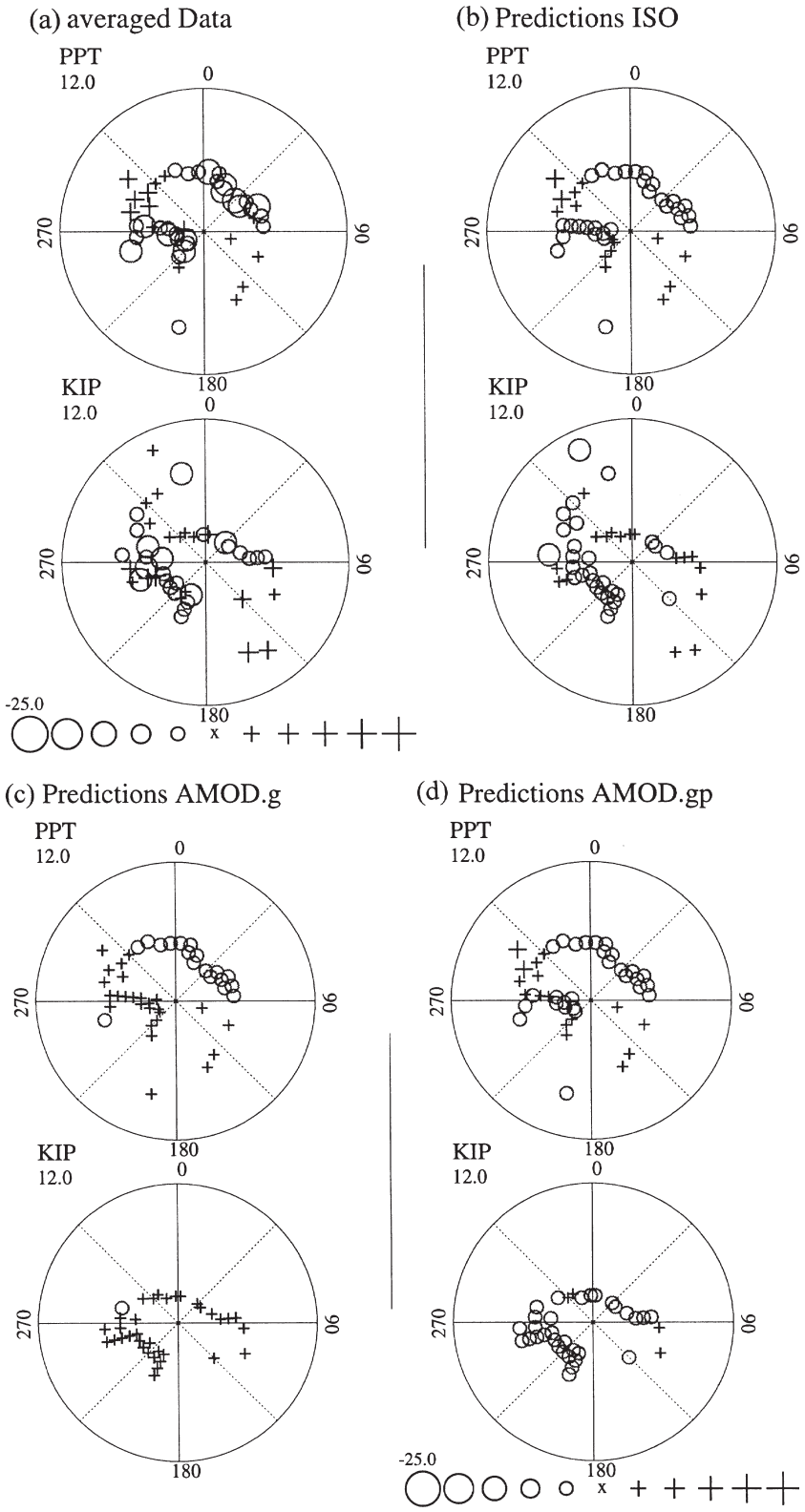

Figure 11. (a) Arrival angles measured for R_1 at 12 mHz at stations KIP and PPT. The angles are plotted as a function of azimuth and epicentral distance (the circle is 180° distance). The data have been slightly smoothed and corrected for possible misalignment of the horizontal components ($-5°$ at PPT, $+2°$ at KIP). (b) Arrival angles predicted by isotropic map ISO of Fig. 1. (c) Arrival angles predicted by anisotropic model AMOD.g. (d) The angles predicted by anisotropic model AMOD.gp. The data at KIP are clearly inconsistent with the predictions of AMOD.g.

GJI000 17/2/98 16:40:46 3B2 version 5.20
The Charlesworth Group, Huddersfield 01484 517077

There is no significant difference in the fit to the polarization data achieved by the two models ISO and AMOD.gp, the isotropic model expanded up to $l=24$ or the anisotropic model with expansions of $l=16$ (0Ψ part) and $l=12$ (2Ψ part). We have shown that our polarization data actually require isotropic phase velocity structure above $l=16$ to be well fit (Laske & Masters 1996). It is likely that polarization data need both short-wavelength isotropic structure and long-wavelength anisotropic structure at the same time to improve the fit further.

In order to obtain accurate high-resolution dispersion maps, and eventually a detailed image of the Earth's anisotropic upper mantle, careful investigation of the possible bias caused by unmodelled effects is necessary. For example, before we include polarization data in the modelling process, we correct for possible errors in the instrument calibration which lead to an apparent rotation of the horizontal components. These rotation angles are approximately -5° and $+1.8^\circ$ at stations PPT and KIP (Laske 1995). Whilst -5° at PPT has been confirmed by the operators as true misrotation of the horizontal components, the observation at KIP is as yet unexplained. It turns out that the average of the polarization angles at this station, predicted by anisotropic map AMOD.g (phase data only) is $+1.1^\circ$. This is the highest non-zero average value for any individual station predicted by any phase-velocity map in our entire data set (the average value is usually 0.2° or less). This is somewhat surprising, since we expect the mean to be close to zero if the azimuthal data coverage is as good as it is for KIP. For the data at this particular station, the rather high non-zero mean of the predictions would account for a significant amount of the signal in the data (about 10 per cent) if the apparent rotation of 1.8° was not removed from the data before the analysis. If the apparent rotation is not removed, the resulting map still shows the rather peculiar pattern of anisotropy around Hawaii, though it appears to be somewhat weaker. We conclude from this that we obviously need to investigate trends in our data very carefully in order to obtain an accurate map of the global distribution of anisotropic phase velocity.

It is also worth noting that although the contribution of the 4Ψ terms is expected to be small for Rayleigh waves for realistic petrological models, we do not observe this with our current data set. If the 4Ψ terms are included in the inversion, their spherical harmonic coefficients are almost as large as those for the 2Ψ terms. Our current data set certainly cannot constrain all the model parameters so that structure from one set of coefficients may be mapped into another. However, we expect that with the recent rapid expansion of the global networks, the resolution in our global dispersion maps will be greatly improved so that a more systematic examination lies within our reach.

To summarize, this study has shown that polarization data have the potential for improving the recovery of anisotropic structure by diminishing the trade-off between isotropic and anisotropic effects. If anisotropy is not much stronger that what is commonly found in the literature, linear perturbation theory is accurate enough to interpret such data in terms of weakly anisotropic lateral phase-velocity heterogeneity, and inclusion of such data in a linear inversion becomes straightforward. We want to stress, however, that careful analysis of such data is required in order to avoid bias introduced by sources which do not affect the phase data.

ACKNOWLEDGMENTS

We wish to thank the GEOSCOPE project team at Institute Physique de Globe de Paris, the IDA project team at IGPP, La Jolla, the USGS team at ASL, and the IRIS-DMC for the easily accessible, high-quality data used in this study. We also wish to thank Jean-Paul Montagner, Jeannot Trampert, Yu-Shen Zhang and Göran Ekström for making available their phase-velocity maps. This research was financed by National Science Foundation grants EAR-93-04194 and EAR-94-18063.

REFERENCES

Ansel, V. & Nataf, H.-C., 1989. Anisotropy beneath 9 stations of the GEOSCOPE broadband network as deduced from shear-wave splitting, *Geophys. Res. Let.,* **16,** 409–412.

Backus, G.E., 1962. Long-wave elastic anisotropy produced by horizontal layering, *J. geophys. Res.,* **67,** 4427–4440.

Backus, G.E., 1965. Possible forms of seismic anisotropy of the uppermost mantle under oceans, *J. geophys. Res.,* **70,** 3429–3439.

Constable, S.C., Parker, R.L. & Constable, C.G., 1987. Occam's inversion: a practical algorithm for generating smooth models from electromagnetic sounding data, *Geophysics,* **52,** 289–300.

Crampin, S., 1975. Distinctive particle motion of surface waves as a diagnostic of anisotropic layering, *Geophys. J. R. astr. Soc.,* **40,** 177–186.

Crampin, S. & Booth, D.C., 1985. Shear-wave polarizations near the North Anatolian Fault, II, Interpretation in terms of crack-induced anisotropy, *Geophys. J. R. astr. Soc.,* **83,** 75–92.

Dziewonski, A.M. & Anderson, D.L., 1981. Preliminary reference earth model, *Phys. Earth planet. Inter.,* **25,** 297–356.

Ekström, G., Tromp, J. & Larson, E., 1997. Measurements and global models of surface wave propagation, *J. geophys. Res.,* **102,** 8137–8157.

Forsyth, D.W., 1975. The early structural evolution and anisotropy of the oceanic upper mantle, *Geophys. J. R. astr. Soc.,* **43,** 103–162.

Forsyth, D.W., Dorman, L.M., Phipps-Morgan, J. & Shen, Y., 1996. Anisotropy and lateral variations in shear wave velocity from propagation of Rayleigh waves across the MELT array, *EOS, Trans. Am. geophys. Un.,* **77,** F652–F653.

Fuchs, K., 1983. Recently formed elastic anisotropy and petrological models for the continental subcrustal lithosphere in southern Germany, *Phys. Earth planet. Inter.,* **31,** 93–118.

Gilbert, F. & Dziewonski, A.M., 1975. An application of normal mode theory to the retrieval of structural parameters and source mechanisms from seismic spectra, *Phil. Trans. R. Soc. Lond.,* A, **278,** 187–269.

Grünewald, M., 1988. Effects of anisotropy in southwest Germany on the propagation of surface waves, *Phys. Earth planet. Inter.,* **51,** 42–54.

Kawasaki, I., 1986. Azimuthally anisotropic model of the oceanic upper mantle, *Phys. Earth planet. Int.,* **43,** 1–21.

Kendall, J.-M., 1994. Teleseismic arrivals at a mid-ocean ridge: effects of mantle melt and anisotropy, *Geophys. Res. Let.,* **21,** 301–304.

Laske, G., 1995. Global observation of off-great circle propagation of long-period surface waves, *Geophys. J. Int.,* **123,** 245–259.

Laske, G. & Masters, G., 1996. Constraints on global phase velocity maps by long-period polarization data, *J. geophys. Res.,* **101,** 16 059–16 075.

Laske, G., Masters, G. & Zürn, W., 1994. Frequency-dependent polarization measurements of long-period surface waves and their implications for global phase velocity maps, *Phys. Earth planet. Inter.,* **84,** 111–137.

Maupin, V., 1985. Partial derivatives of surface wave phase velocities for flat anisotropic structures, *Geophys. J. R. astr. Soc.,* **83,** 379–385.

Maupin, V., 1987. Etude des characteristiques des ondes de surface en milieu anisotrope: application a l'analyse d'anomalies de polarization a la station do Port-aux-francais, *PhD thesis,* Université Louis Pasteur, Strasbourg, France.

Mitchell, B.J., 1984. On the inversion of Love and Rayleigh wave dispersion and implications for earth structure and anisotropy, *Geophys. J. R. astr. Soc.,* **76,** 233–241.

Mochizuki, E., 1990. Simple formulae for path and amplitude anomalies of anisotropic surface waves, *Geophys. J. Int.,* **102,** 263–264.

Montagner, J.-P. & Anderson, D.L., 1989. Constrained reference mantle model, *Phys. Earth planet. Inter.,* **58,** 205–227.

Montagner, J.-P. & Nataf, H.-C., 1986. A simple method for inverting the azimuthal anisotropy of surface waves, *J. geophys. Res.,* **91,** 511–520.

Montagner, J.-P. & Tanimoto, T., 1990. Global anisotropy in the upper mantle inferred from the regionalization of phase velocities, *J. geophys. Res.,* **95,** 4797–4819.

Montagner, J.-P. & Tanimoto, T., 1991. Global upper mantle tomography of seismic velocities and anisotropies, *J. geophys. Res.,* **96,** 20 337–20 351.

Nishimura, C.E. & Forsyth, D.W., 1989. The anisotropic structure of the upper mantle in the Pacific, *Geophys. J.,* **96,** 203–229.

Park, J. & Yu, Y., 1992. Anisotropy and coupled free oscillations: simplified models and surface wave observations, *Geophys. J. Int.,* **110,** 401–420.

Raitt, R.W., Shor, G.G., Jr., Francis, T.J.G. & Morris, G.B., 1969. Anisotropy of the Pacific upper mantle, *J. geophys. Res.,* **74,** 3095–3109.

Regan, J. & Anderson, D.L., 1984. Anisotropic models of the upper mantle, *Phys. Earth planet. Inter.,* **35,** 227–263.

Schlue, J.W., 1977. A physical model for surface wave azimuthal anisotropy, *Bull. seism. Soc. Am.,* **67,** 1515–1519.

Schlue, J.W. & Knopoff, L., 1976. Shear wave anisotropy in the upper mantle of the Pacific Basin, *Geophys. Res. Lett.,* **3,** 359–362.

Smith, M.L. & Dahlen, F.A., 1973. The azimuthal dependence of Love and Rayleigh wave propagation in a slightly anisotropic medium, *J. geophys. Res.,* **78,** 3321–3333.

Snieder, R., 1986. The influence of topography on the propagation and scattering of surface waves, *Phys. Earth planet. Inter.,* **44,** 226–241.

Suetsugu, D. & Nakanishi, I., 1987. Three-dimensional velocity map of the upper mantle beneath the Pacific Ocean as determined from Rayleigh wave dispersion, *Phys. Earth planet. Inter.,* **47,** 205–229.

Tanimoto, T., 1987. Surface-wave ray tracing equations and Fermat's principle in an anisotropic earth, *Geophys. J. R. astr. Soc.,* **88,** 231–240.

Tanimoto, T. & Anderson, D.L., 1985. Lateral heterogeneity and azimuthal anisotropy of the upper mantle: Love and Rayleigh waves 100–250 s, *J. geophys. Res.,* **90,** 1842–1858.

Trampert, J. & Woodhouse, J.H., 1995. Global phase velocity maps of Love and Rayleigh waves between 40 and 150 seconds, *Geophys. J. Int.,* **122,** 675–690.

Vig, P.K. & Mitchell, B.J., 1990. Anisotropy beneath Hawaii from surface wave particle motion observations, *Pageoph.,* **133,** 1–22.

Vinnik, L.P., Farra, V. & Romanowicz, B., 1989. Azimuthal anisotropy in the Earth from observations of *SKS* at GEOSCOPE and NARS broadband stations, *Bull. seism. Soc. Am.,* **79,** 1542–1558.

Woodhouse, J.H. & Dahlen, F.A., 1978. The effect of a general aspherical perturbation on the free oscillations of the Earth, *Geophys. J. R. astr. Soc.,* **53,** 335–354.

Woodhouse, J.H. & Wong, Y.K., 1986. Amplitude, phase and path anomalies of mantle waves, *Geophys. J. R. astr. Soc.,* **87,** 753–773.

Yu, G.-K. & Mitchell, B.J., 1979. Regionalized shear velocity models of the Pacific upper mantle from observed Love and Rayleigh wave dispersion, *Geophys. J. R. astr. Soc.,* **57,** 311–341.

Yu, Y. & Park, J., 1994. Hunting for azimuthal anisotropy beneath the Pacific Ocean region, *J. geophys. Res.,* **99,** 15 399–15 421.

Zhang, Y.-S. & Lay, T., 1996. Global surface-wave phase velocity variations, *J. geophys. Res.,* **101,** 8415–8436.

Zhang, Y.-S. & Tanimoto, T., 1993. High-resolution global upper mantle structure and plate tectonics, *J. geophys. Res.,* **98,** 9793–9823.

GJI000 17/2/98 16:41:01 3B2 version 5.20
The Charlesworth Group, Huddersfield 01484 517077